Biochemical and mass spectrometric characterization of soluble ecto-5′-nucleotidase from bull seminal plasma

Carlo FINI*†[1,2], Fabio TALAMO‡[1], Silvia CHERRI*, Marcello COLI*, Ardesio FLORIDI*, Lino FERRARA‡ and Andrea SCALONI‡

*Dipartimento di Medicina Interna, Università di Perugia, via del Giochetto 6, 06126 Perugia, Italy, †I.N.F.M., Unità di Viterbo, Largo dell'Università, 01100 Viterbo, Italy, and ‡Proteomics and Mass Spectrometry Laboratory, I.S.P.A.A.M., National Research Council, via Argine 1085, 80147 Napoli, Italy

Ecto-5′-nucleotidase (ecto-5′-NT) is a glycosylphosphatidylinositol-anchored membrane-bound protein that is ubiquitous in mammalian tissues. It is a target for a number of therapeutic drugs since increased levels of the enzyme correlate with various disease states. In this investigation, we describe the properties of a soluble ecto-5′-NT derived from bull seminal plasma. The protein was highly heterogeneous as demonstrated by chromatofocusing and two-dimensional PAGE. Sequencing analyses revealed a truncated polypeptide lacking the glycosylphospatidylinositol attachment site, suggesting that it is produced post-translationally by cleavage at Gln^{547} and/or Phe^{548}. Heterogeneity was largely due to differential glycosylation, especially in the oligosaccharides linked to Asn^{403}. Significant differences in substrate specificity were observed between isoforms and, on the basis of molecular-modelling studies, were interpreted in terms of variable glycosylation causing steric hindrance of the substrate-binding site. Thus the soluble forms of ecto-5′-NT found in bull seminal plasma are unique both biochemically and structurally, and have a putative role in signalling interactions with spermatozoa following ejaculation and capacitation in the female reproductive tract.

Key words: glycosylphosphatidylinositol anchor, MS, membrane, soluble ecto-5′-nucleotidase.

INTRODUCTION

Ecto-5′-nucleotidase (ecto-5′-NT; EC 3.1.3.5) catalyses the hydrolysis of nucleoside 5′-monophosphates to the corresponding nucleosides and inorganic phosphate. It is ubiquitous in tissues and is involved intimately over a range of physiological processes ensuring the extracellular hydrolysis of 5′-AMP to adenosine [1]. The action of a number of therapeutic drugs can be explained by direct stimulation/inhibition of 5′-NT activity. Thus, in the rat heart, increased levels of adenosine following histamine treatment have been causally related to activation of ecto-5′-NT [2]. Similarly, in comparing the effects of nicorandil and glibenclamide, two KATP channel openers, it was observed in rat heart that only nicorandil increased the interstitial level of adenosine via activation of ecto-5′-NT and cGMP pathways [3]. Increased adenosine levels, however, are not always associated with ecto-5′-NT stimulation as shown following chronic salt loading in renal cortex and medulla cells [4]. Differential effects of clozapine and haloperidol on the purinergic system have also been explained in terms of their effects on ecto-5′-NT [5].

The above-mentioned activities have always been ascribed to the action of an ecto-5′-NT linked to the plasma membrane through a glycosylphospatidylinositol (GPI) anchor. However, a 'soluble' form of ecto-5′-NT has also been described in synovial fluid [6] and human placenta [7]. This species seemed to be generated from the hydrolysis of the GPI anchor, catalysed by phosphatidylinositol-specific phospholipase C (PI-PLC), as shown by similarities in the N-terminal sequence, apparent molecular mass, low K_m values towards AMP and enzyme-specific inhibition by nucleoside di- and triphosphates [7]. From a comparative study of the catalytic properties of three forms of the enzyme, namely, native ecto-5′-NT linked to the plasma membrane of pig lymphocytes, the solubilized form obtained after treatment with PI-PLC and the purified GPI-ecto-5′-NT reconstituted in liposomes with different lipid composition, it was found that anchoring of the protein to the lipid bilayer by the GPI moiety influenced strongly the catalytic efficiency of the enzyme [8]. However, an extensive study on the naturally occurring form of soluble ecto-5′-NT has not been performed so far.

In the present study, we report the purification of the soluble form of ecto-5′-NT from bull seminal plasma and its structural characterization by MS procedures. The purified enzyme was resolved into several isoforms differing in their glycosidic moiety as well as substrate specificity. In all species, the GPI anchor was absent and the nature of the C-terminal peptide suggested processing by a C-terminal peptidase.

EXPERIMENTAL

Materials

Trypsin, CNBr and α-cyano-4-hydroxy-cinnamic acid were purchased from Sigma. Polybuffer exchanger PBE 94 and PBE 74 amphoteric buffer were purchased from Amersham Pharmacia Biotech (Piscataway, NJ, U.S.A.). All other reagents and solvents were of HPLC grade from Fluka (Buchs, Switzerland).

Purification of soluble ecto-5′-NT

Bull semen samples, usually 200 ml after liquefaction, were centrifuged at 800 ***g*** for 10 min at 4 °C to separate the spermatozoa. The supernatant (seminal plasma) was recentrifuged at 105 000 ***g*** for 2 h at 4 °C. The pellet was discarded and the supernatant was dialysed overnight against 50 mM Tris/HCl buffer (pH 8.0), containing 1 mM NaCl, 0.1 mM protease inhibitor cocktail

Abbreviations used: GPI, glycosylphospatidylinositol; IEF, isoelectric focusing; MALDI, matrix-assisted laser-desorption ionization; ecto-5′-NT, ecto-5′-nucleotidase; 5′-NT, 5′-nucleotidase; PI-PLC, phosphatidylinositol-specific phospholipase C; RP, reverse phase.

[1] These authors have contributed equally to this work.

[2] To whom correspondence should be addressed (e-mail cfini@unipg.it).

(antipain, chymostatin, EDTA and Pefabloc® SC) and 0.02 % sodium azide. Thereafter, chromatographic procedures for the purification of the soluble form of ecto-5′-NT were similar to those described previously for the GPI-anchored 5′-NT from bull seminal plasma [9] except that detergents were omitted from the buffers. The main steps were ion exchange on DEAE A50 followed by affinity chromatography on concanavalin A–Sepharose and AMP–agarose. Typically, 200 ml of bull seminal plasma yielded 7 mg of soluble 5′-NT containing approx. 300 units/mg. Protein quantification was performed by means of the bicinchoninic acid protein assay reagent kit (Pierce, Rockford, IL, U.S.A.) with BSA as a standard, and the enzyme activity was estimated as described previously using AMP, IMP, GMP and dCMP as substrates [10]. One unit of activity corresponded to the formation of 1 μmol of inorganic phosphate per min at 37 °C.

For gel-filtration experiments, samples of electrophoretically homogeneous 5′-NT stored in 10 mM imidazole (pH 6.8), also containing 1 mM β-glycerophosphate, 75 mM NaCl and 1 mM sodium azide, were dialysed against 50 mM Tris/HCl (pH 7.5). The dialysed samples were applied to a column of Sephacryl S-300 (46 cm × 1.6 cm), equilibrated previously with the same buffer. Elution was performed at a flow rate of 0.25 ml/min at 4 °C.

UV–Vis absorbance spectra

Spectra were recorded by using a set of matched quartz cells (1 cm) on a Jasco model V550 UV/Vis double-beam spectrophotometer equipped with a Peltier temperature control device. The internal temperature of the sample cell was 25 ± 0.1 °C. Spectra were recorded from 450 to 235 nm at a bandwidth of 1 nm and processed with Jasco software. Solutions examined were degassed under vacuum and their protein content was approx. 0.4 mg/ml in Tris/HCl (pH 8.0).

Chromatofocusing

Protein samples (0.3 mg/ml) were loaded on to a column packed with PBE 94 gel (54 cm × 1.2 cm), equilibrated with 25 mM imidazole (pH 7.4). Elution was performed with Polybuffer PBE 74 (pH 5.0). The flow rate was 0.27 ml/min; fractions of 1 ml were collected and assayed for 5′-NT activity, as described above.

Gel electrophoresis and image analysis

SDS/PAGE was performed in Mini-Protean II cells (Bio-Rad, Richmond, CA, U.S.A.) at 60 mA constant current, 10 % (w/v) acrylamide and the gel thickness was 1.0 mm. Silver staining was performed as described by Shevchenko et al. [11].

A sample containing 10 μg of total protein was separated in a horizontal two-dimensional electrophoresis set-up (Multiphor II; Amersham Pharmacia, Frieburg, Germany) as described by Gorg et al. [12]. Isoelectric focusing (IEF) was performed on immobilized pH gradient device strips (0.5 mm × 170 mm), containing Immobilines NL 3–10. After equilibration, the IPG-gel strips were transferred on to two-dimensional vertical gradient slab gels [9–16 % (w/v) of total monomer (acrylamide + *N*,*N*′-methylene-bis-acrylamide) in solution] and run with the Laemmli-SDS-discontinuous system [13]. Protein was visualized by silver staining [11].

Fractions from chromatofocusing were analysed by polyacrylamide IEF as described previously in [14]. A pH gradient was obtained by mixing ampholytes over the pH range 4–6, 5–7 and 6–8 (Pharmacia Biotech, Peapack, NJ, U.S.A.) in the presence of 10 % (v/v) glycerin (Merck, Darmstadt, Germany). Catolyte was 1 M NaOH and anolyte was 1 M phosphoric acid.

Gels were scanned using a GS-710 Imaging Densitometer (Bio-Rad) linked to Macintosh computers. Image computer analysis was performed using the Melanie 2 software package [15].

Protein digestion and peptide purification

Protein samples from isochromatofocusing were digested either with CNBr in 70 % (v/v) trifluoroacetic acid or with trypsin (E : S 1 : 100) in 1 M urea, 25 mM ammonium bicarbonate (pH 8), at 37 °C, overnight. Peptide mixtures were analysed directly with the mass spectrometer following ZipTipC_{18} desalting or separated by reverse phase (RP)-HPLC on a Vydac C_{18} column 218TP52 (250 mm × 1 mm), 5 μm, 300 Å (1 Å = 10^{-10} m) pore size (The Separation Group, Hesperia, CA, U.S.A.), using a linear gradient from 5 to 60 % of acetonitrile in 0.1 % trifluoroacetic acid over 60 min, at the flow rate of 60 μl/min. Individual components were collected manually and freeze-dried.

MS analysis and peptide sequencing

Matrix-assisted laser-desorption ionization (MALDI) mass spectra were recorded using a Voyager DE-PRO mass spectrometer (Applied Biosystems, Foster City, CA, U.S.A.) as described previously [16]; a mixture of analyte solution and α-cyano-4-hydroxy-cinnamic acid was applied to the sample plate and dried. Mass calibration was performed using the molecular ions from peptides produced by protease autoproteolysis and/or the matrix as internal standards. Spectra were recorded in positive and negative polarity by using the instrument either in linear (glycopeptides) and/or reflectron mode (peptides). Assignments of the recorded mass values to individual peptides were performed on the basis of their molecular mass and protease/reagent specificity. Peptide numbering was according to the 5′-NT unprocessed precursor.

Peptide fractions were also analysed by using a Procise 491 protein sequencer (Applied Biosystems), equipped with a 140 C microgradient apparatus and a 785A UV detector (Applied Biosystems) for the automated identification of phenylthiohydantoin amino acids. Possible mixed peptide sequence data were sorted and matched to the 5′-NT sequence with the FASTF or TFASTF algorithms [17].

Molecular modelling

A three-dimensional model of bovine 5′-NT was constructed on the basis of the crystallographic structures of 5′-NT from *Escherichia coli* (PDB code 1USH, 2USH, 1HO5 and 1HPU) taken from the Protein Data Bank (Brookhaven National Laboratory, Upton, NY, U.S.A.). Sequence analysis was performed using the BLASTP2 algorithm in the EXNRL-3D database. Structure-based sequence alignment was obtained by using the program AMPS [18] with secondary structure-dependent gap penalties [19]. Computer modelling was performed on a Silicon Graphics O2 workstation. The model included those residues occurring in the processed polypeptide chain (residues 27–549) and was constructed with the Insight/Homology program package (Biosym Technologies, San Diego, CA, U.S.A.). Several cycles of constrained energy minimization regularized the structure and geometrical parameters. The final structure was validated by using the WHATCHECK program [20]. Figure 6 was drawn using the Swiss-PDBviewer [21].

Table 1 Purification of soluble ecto-5′-NT from bull seminal plasma

Step	Total protein (mg)	Total activity (units)	Specific activity (units/mg)	Purification factor	Yield (%)
Supernatant centrifuged at 105 000 ***g***	8000.0	3000.0	0.4	1.0	100.0
DEAE	2400.0	1888.0	0.8	2.1	62.9
Concanavalin A–Sepharose	63.0	1300.0	20.6	55.7	43.3
AMP–agarose	3.5	1050.0	300.0	810.8	35.0

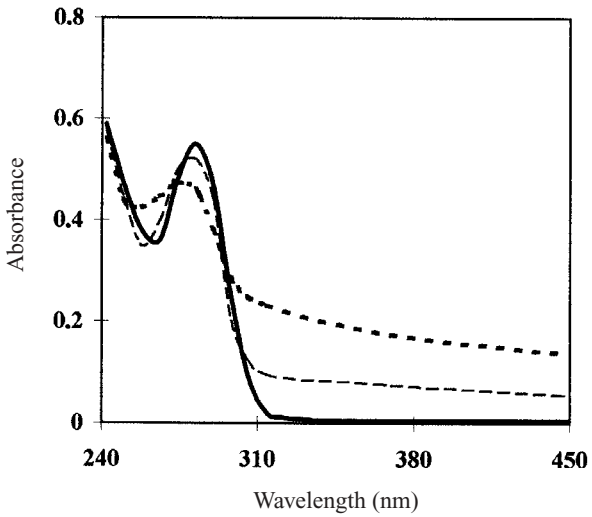

Figure 1 Absorption spectra of soluble ecto-5′-NT

Purified protein preparation obtained as described in the Experimental section (dotted line), first peak of the gel-filtration chromatography shown in Figure 2 after treatment with 20 mM sodium cholate (dashed line), second peak of chromatogram shown in Figure 2 (solid line). Experimental conditions for recording the spectra are described in the Experimental section.

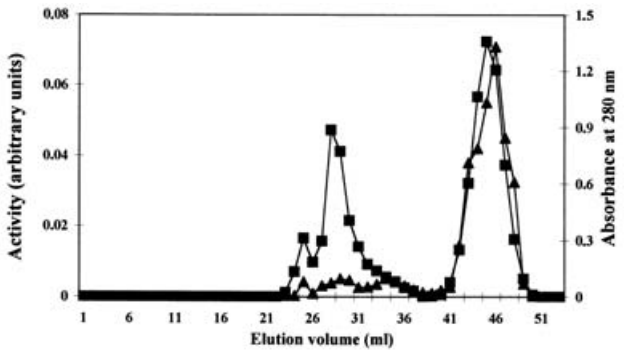

Figure 2 Sephacryl S-300 gel-filtration chromatography of the purified soluble ecto-5′-NT from bull seminal plasma

Experimental conditions are described in the Experimental section. ■, enzymic activity; ▲, absorbance.

RESULTS

Purification and biochemical properties of soluble ecto-5′-NT

Results of the purification method are summarized in Table 1. The scheme has been adapted in different laboratories with modifications to the isolation of ecto-5′-NT from various sources and appears to be unsuitable for the purification of the two cytosolic forms (cN-I the cytosolic 5′-NT preferring AMP and cN-II the cytosolic 5′-NT preferring IMP) of the enzyme. Soluble ecto-5′-NT appeared to prefer IMP over AMP: specific activity 300 versus 156 units/mg respectively. A silver-stained SDS/PAGE of the purified enzyme indicated a single band with a molecular mass of 66.2 kDa (results not shown). Automated Edman degradation analysis of an electroblotted sample gave an N-terminal sequence of WELTILHTNDV . . . , confirming the identity of the protein as ecto-5′-NT.

Aromatic amino acid residues are responsible for protein absorbance in the 230–300 nm region and the occurrence of a sloping baseline in the 310–400 nm range has been attributed to the light scattering contribution due to molecular aggregation phenomena [22]. Since a sloping baseline was evident in the spectral region above 310 nm with our homogeneous 5′-NT preparation (see Figure 1, dotted line), molecular aggregates were separated by gel-filtration chromatography. The elution pattern obtained is shown in Figure 2. AMPase activity was fractionated into two separate peaks. The first peak corresponded to a molecular species of approx. 900 kDa and the second one to a component of approx. 200 kDa. Approximately 30 % of the total eluted protein and approx. 10 % of AMPase activity was present in peak 1 and the remainder in peak 2. Specific activities of the proteins eluted under peaks 1 and 2 were 36 and 156 units/mg respectively. This finding indicated that molecular aggregation of 5′-NT is accompanied by a significant decrease in the AMPase activity, probably due to denaturation. The absorbance spectrum of peak 1 had a sloping baseline similar to that observed for the purified protein before gel filtration (results not shown). The absorbance spectrum of peak 2 (represented by the solid line in Figure 1), however, contained a relatively flat baseline, suggesting that protein aggregation had not occurred in this sample. The spectrum of peak 2 also showed a red-shift of approx. 4 nm with respect to that of the aggregated protein. Moreover, on the basis of gel-filtration chromatography results, it could be deduced that the molecular mass of the 5′-NT of peak 2 would correspond to a trimer of the 66.2 kDa species observed by SDS/PAGE.

In an attempt to release the supposed molecular aggregation, the sample of peak 1 was treated with 20 mM sodium cholate and the spectrum is represented by the broken line in Figure 1. A sloping baseline in the 310–400 nm region was still present and AMPase activity was not increased significantly, indicating that the partial disaggregation of the molecular species could not restore enzymic activity.

A sample of peak 2 was also analysed by two-dimensional-PAGE to ascertain the degree of charge heterogeneity due to post-translational modifications. A typical array of closely spaced spots was observed in the gel indicating at least 14 different species (results not shown).

Purification of the different ecto-5′-NT species visualized by two-dimensional-PAGE was performed by chromatofocusing. This technique allowed the separation of four main peaks (5′-NT-1, 5′-NT-2, 5′-NT-3 and 5′-NT-4), eluting at pH values of 6.48, 6.33, 6.19 and 6.07 respectively (Figure 3A). Each peak was further characterized by IEF (Figure 3B); as expected this analysis revealed the occurrence of several species in each

Table 2 Best substrate determination for the soluble ecto-5′-nucleotidase peaks obtained following chromatofocusing separation

V_{max}/K_m ratios are reported. K_m and V_{max} values (means ± S.D. for seven experiments) were calculated by using the computer program ENZPACK3 (Biosoft, Cambridge, U.K.) and the method of Eadie–Hofstee. The statistical significance at the 0.1 % level of the differences between the V_{max}/K_m values for the different 5′-NT samples with the same substrate, as well as for the same 5′-NT with different substrates, was estimated by the *t* test of significance. Calculations were performed using the computer program ORIGIN 5.0 (Microcal Software, Northampton, MA, U.S.A.).

	5′-NT-1			5′-NT-2			5′-NT-3			5′-NT-4		
Substrate	V_{max}	K_m	V_{max}/K_m	V_{max}	K_m	V_{max}/K_m	V_{max}	K_m	V_{max}/K_m	V_{max}	K_m	V_{max}/K_m
AMP	4.48 ± 0.29	0.11 ± 0.005	40.72 ± 5.95	38.35 ± 6.05	0.06 ± 0.006	641.66 ± 15.96	37.95 ± 5.09	0.11 ± 0.005	345.00 ± 13.23	27.35 ± 2.85	0.06 ± 0.006	455.83 ± 17.79
IMP	8.15 ± 0.45	0.15 ± 0.006	54.33 ± 5.45	60.52 ± 5.04	0.07 ± 0.007	864.57 ± 29.32	47.85 ± 3.19	0.06 ± 0.004	797.50 ± 17.05	42.52 ± 5.22	0.07 ± 0.007	607.43 ± 14.24
GMP	8.76 ± 0.39	0.22 ± 0.012	39.81 ± 4.58	96.32 ± 5.35	0.09 ± 0.009	1070.22 ± 59.87	50.40 ± 2.72	0.16 ± 0.007	315.00 ± 12.50	57.12 ± 6.20	0.07 ± 0.007	816.00 ± 30.56
dCMP	1.31 ± 0.06	0.05 ± 0.004	26.20 ± 2.78	3.20 ± 0.27	0.04 ± 0.003	80.00 ± 5.76	5.20 ± 0.74	0.03 ± 0.003	173.33 ± 11.86	7.62 ± 0.45	0.06 ± 0.008	127.00 ± 18.76

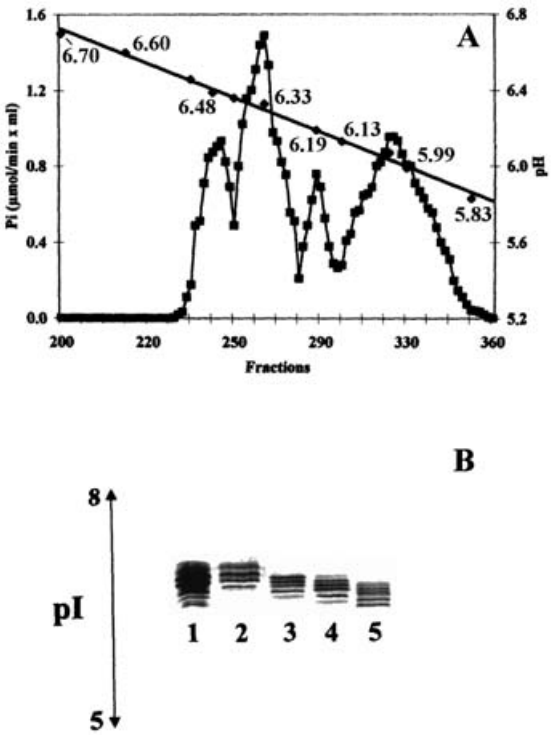

Figure 3 pI-dependent separation of soluble 5′-NT

The purified enzyme was resolved by isochromatofocusing as described in the Experimental section (**A**). Peaks 1, 2, 3 and 4 from left correspond to 5′-NT-1, 5′-NT-2, 5′-NT-3 and 5′-NT-4 respectively. ■, enzymic activity; ◆, pH gradient values. Each purified fraction was analysed by IEF (**B**); lane 1, ecto-5′-NT; lane 2, 5′-NT-1; lane 3, 5′-NT-2; lane 4, 5′-NT-3; lane 5, 5′-NT-4 respectively.

collected fraction with a progressive increase in components with lower pI values arising from 5′-NT-1 to 5′-NT-4.

Fractions from each chromatofocusing peak were collected and their protein content and AMPase activity measured. The specific activities, measured using 5′-AMP as a substrate, were 9.12, 100.00, 337.70 and 36.10 units/mg for 5′-NT-1, 5′-NT-2, 5′-NT-3 and 5′-NT-4 respectively. Ecto-5′-NT from different sources have always shown preference for AMP and its K_m values have been found in the low micromolar range, with typical hyperbolic *v*/[S] diagrams (Michaelis–Menten kinetics). Direct plots of initial reaction velocity versus substrate concentration for the species recovered from chromatofocusing were plotted and relevant V_{max}/K_m ratios were calculated (Table 2). Isoforms 2 and 4 appeared to prefer GMP. Isoform 3 was slightly more active towards IMP, whereas AMP did not seem to be the preferred substrate in any case. K_m values for ribonucleotides were in the micromolar range (50–200 μM), always higher than those determined for ecto-5′-NT containing its GPI anchor (11 μM). The AMPase activities of all the four forms were inhibited by ATP as well as α,β-methyleneadenosine 5′-diphosphate, a specific powerful inhibitor of ecto-5′-NT (results not shown).

Structural characterization of soluble ecto-5′-NT

Protein samples from isochromatofocusing were hydrolysed with CNBr as reported in the Experimental section, and the resulting peptide mixtures were analysed directly by MALDI-MS. The spectra obtained for 5′-NT-1, 5′-NT-2, 5′-NT-3 and 5′-NT-4 were very similar and showed common signals which could

Table 3 MALDI-MS and sequence analysis of the RP-HPLC-purified C-terminal peptides occurring in the CNBr hydrolysates of soluble and non-soluble ecto-5′-NT species

Edman degradation was performed on peptide fractions from all five 5′-NT samples, always producing the same amino acid sequence reported below. EtNP, phosphoethanolamine; GlcN, glucosamine; HexNAc, *N*-acetyl-hexosamine; InoP, inositol phosphate; Man, mannose. The observed signals of the membrane-bound 5′-NT were interpreted according to Taguchi et al. [23].

5′-NT-1 MH^+	5′-NT-2 MH^+	5′-NT-3 MH^+	5′-NT-4 MH^+	Non-soluble 5′-NT MH^+	Sequence analysis	Structure
1371.75	1371.76	1371.77	1371.76	–		(536–547)
1518.85	1518.87	1518.87	1518.89	–		(536–548)
1605.89	1605.88	1605.87	1605.90	–	KVLYPAVEGRIQF	(536–549)
–	–	–	–	2742.89		(536–549)-$(EtNP)_2$-$(Man)_3$-GlcN-InoP
–	–	–	–	2904.92		(536–549)-$(EtNP)_2$-$(Man)_4$-GlcN-InoP
–	–	–	–	2945.95		(536–549)-$(EtNP)_2$-$(Man)_3$-HexNAc-GlcN-InoP

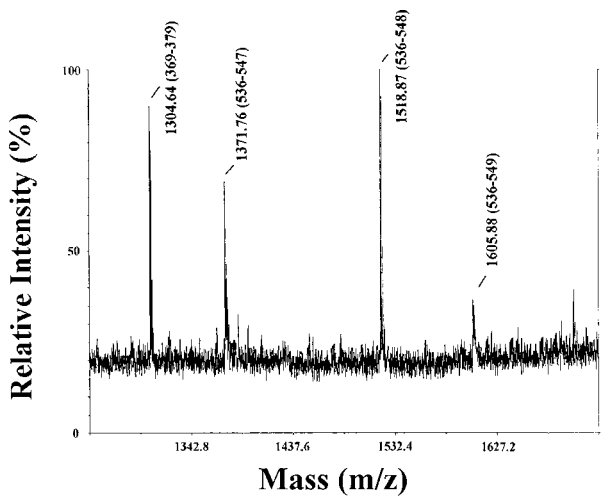

Figure 4 MALDI-MS analysis of 5′-NT-2 following hydrolysis with CNBr

Signals occurring in the spectrum were associated with peptides on the basis of the polypeptide sequence and reagent specificity. Spectra were recorded in positive polarity by using the instrument in reflectron mode. Identical spectra were obtained for 5′-NT-1, 5′-NT-3 and 5′-NT-4.

be associated with the expected peptides on the basis of the 5′-NT sequence and CNBr specificity. However, the analysis showed together the MH^+ at *m/z* 812.39, 836.38, 1304.64, 2252.21 and 2771.44 corresponding to peptides 380–386, 106–113, 369–379, 490–510 and 511–535 respectively, the occurrence of specific signals at *m/z* 1371.76, 1518.87 and 1605.88 (Figure 4) that were associated with truncated (536–547 and 536–548) and not post-translationally modified C-terminal peptide species. Identical results were obtained for 5′-NT-1, 5′-NT-2, 5′-NT-3 and 5′-NT-4. The corresponding analysis of the membrane-bound 5′-NT hydrolysate did not show these peaks. In contrast, the expected signals of the C-terminal peptide bearing inositol phosphoglycans were observed [9,23].

To confirm these observations, a comparative peptide mapping experiment was performed on 5′-NT-1, 5′-NT-2, 5′-NT-3, 5′-NT-4 and membrane-bound 5′-NT CNBr hydrolysates by RP-HPLC. The purified fractions corresponding to the C-terminal peptide species were then subjected to automated Edman degradation and MALDI-MS analysis. The results are summarized in Table 3 and demonstrate conclusively that these forms of soluble 5′-NT did not contain the GPI anchor but were mainly hydrolysed at the C-terminus, specifically at the level of Gln^{547} and Phe^{548}.

To characterize completely the post-translational modifications occurring on these 5′-NT forms, protein samples were digested with trypsin under mild denaturing conditions. These digests were resolved by RP-HPLC, and the collected peptide fractions were submitted to MALDI-MS analysis and automated Edman degradation. The results are summarized in Table 4. These experiments, together with the analysis of CNBr hydrolysates, covered approx. 88 % of the entire protein sequence, confirming that C-terminal processing was occurring at Gln^{547} and Phe^{548}. Furthermore, the mass spectra measured for fractions 4, 7 and 24 confirmed the redox state defined previously for the eight cysteine residues present in the polypeptide chain (Cys^{51}-Cys^{57}, Cys^{353}-Cys^{358}, Cys^{365}-Cys^{387} and Cys^{476}-Cys^{479}) [9]. In addition, the occurrence in fractions 4, 8, 11 and 29 of adjacent signals differing by 146, 162, 203 and 291 mass units made glycopeptides recognizable immediately and demonstrated Asn^{53}, Asn^{311}, Asn^{333} and Asn^{403} as sites of N-glycosylation. No signals corresponding to the unglycosylated peptides were present in any of the fractions analysed. On the basis of the known biosynthetic pathway of N-linked oligosaccharides and the molecular mass of the peptide moieties, the signals from the fractions 4, 8 and 11 (common to 5′-NT-1, 5′-NT-2, 5′-NT-3 and 5′-NT-4) were interpreted as peptides spanning residues 51–63, 331–341 and 298–321 respectively, bearing high-mannose-type N-linked glycans. These spectra demonstrated that the nature of the N-linked glycans on Asn^{311} and Asn^{333} were identical with those published previously for the membrane-bound 5′-NT [9]. The glycan occurring at Asn^{53}, however, showed a small number of mannose residues linked to the pentasaccharide core with respect to the membrane-bound enzyme. Comparison of the signals reported in Table 4 demonstrated that no differences were observed among the different 5′-NT forms. The only exception was fraction 29 for which different spectra were recorded for the four 5′-NT species. In fact, the MALDI-MS analysis of this fraction showed significant differences between 5′-NT-1, 5′-NT-2, 5′-NT-3 and 5′-NT-4 (Figure 5). A series of 22 glycopeptide species were identified containing different N-linked high mannose, complex and hybrid structures on Asn^{403}. The glycan composition of each component is reported in Table 5; several glycopeptides were common to all panels reported in Figure 5. However, the number and type of N-linked oligosaccharides were different with respect to those occurring at this site in the membrane-bound enzyme [9]. An increase in sialylated glycans, together with a decrease in high-mannose structures, was observed arising from 5′-NT-1 to 5′-NT-4. This result was not surprising on the basis of the chromatofocusing and IEF results reported in Figure 3, which indicated a progressive decrease in pI from 5′-NT-1 to 5′-NT-4.

Table 4 MALDI-MS and automated Edman degradation analysis of the RP-HPLC-purified peptides occurring in the tryptic digest of the isochromatofocused 5′-NT samples

Hex, hexose; $(Man)_3(GlcNAc)_2$, pentasaccharide core. X indicates amino acid not identified by sequencing.

HPLC peak	5′-NT-1 MH^+	5′-NT-2 MH^+	5′-NT-3 MH^+	5′-NT-4 MH^+	Sequence analysis	Peptide, sugar composition,disulphide, glycosylation site, glycan type
1	572.5	572.7	572.6	572.8	LIAQK	(228–232)
2	1335.9	1335.5	1335.3	1335.7	VPSYEPLRMDK	(481–491)
3	–	961.0	961.1	961.5		(481–488)
4	2506.6	2506.7	2506.6	2506.3		(51–63) + $Hex_2(Man)_3(GlcNAc)_2$, Cys^{51}-Cys^{57}, Asn^{53}, high mannose
	2668.4	2668.8	2668.5	2668.4	XVNASRXVGGVAR	(51–63) + $Hex_3(Man)_3(GlcNAc)_2$, Cys^{51}-Cys^{57}, Asn^{53}, high mannose
	2830.7	2830.3	2830.1	2830.8		(51–63) + $Hex_4(Man)_3(GlcNAc)_2$, Cys^{51}-Cys^{57}, Asn^{53}, high mannose
	2992.3	2992.6	2992.4	2992.9		(51–63) + $Hex_5(Man)_3(GlcNAc)_2$, Cys^{51}-Cys^{57}, Asn^{53}, high mannose
5	1004.5	1004.2	1004.1	1004.3	VLYPAVEGR	(537–545)
6	1245.4	1245.2	1245.6	1245.9		(537–547)
	1392.7	1392.5	1392.4	1392.3	VLYPAVEGRIQF	(537–548)
	1028.3	1028.3	1028.1	1028.7	ISGLYSPYK	(154–162)
7	1063.4	1063.2	1063.6	1063.6	LEVLXTQXR	(472–480), Cys^{476}–Cys^{479}
8	2646.6	2646.3	2646.3	2646.5		(331–341) + $Hex_3(Man)_3(GlcNAc)_2$, Asn^{333}, high mannose
	2808.8	2808.5	2808.6	2808.7	LDXYSTQEL . . .	(331–341) + $Hex_4(Man)_3(GlcNAc)_2$, Asn^{333}, high mannose
	2970.0	2970.4	2970.3	2970.1		(331–341) + $Hex_5(Man)_3(GlcNAc)_2$, Asn^{333}, high mannose
	3132.1	3132.4	3132.7	3132.0		(331–341) + $Hex_6(Man)_3(GlcNAc)_2$, Asn^{333}, high mannose
9	1834.6	1834.8	1834.3	1834.7		(518–534)
	2076.8	2076.2	2076.7	–		(516–534)
10	1179.6	1179.5	–	1179.1		(275–285)
	–	1307.5	1307.3	1307.3		(274–285)
11	3895.7	3895.5	3895.4	3895.7		(298–321) + $Hex_3(Man)_3(GlcNAc)_2$, Asn^{311}, high mannose
	4057.3	4057.2	4057.7	4057.2	GNVVTSHGNPILLXS . . .	(298–321) + $Hex_4(Man)_3(GlcNAc)_2$, Asn^{311}, high mannose
	4219.4	4219.2	4219.3	4219.7		(298–321) + $Hex_5(Man)_3(GlcNAc)_2$, Asn^{311}, high mannose
	4380.7	4380.4	4380.6	4380.3		(298–321) + $Hex_6(Man)_3(GlcNAc)_2$, Asn^{311}, high mannose
12	2246.4	2246.3	2246.1	2246.7	GVDVVVGGHSNT . . .	(235–256)
13	1852.3	1852.0	1852.6	–	EVPAGQYPFIVTS . . .	(257–273)
	–	1980.2	1980.7	1980.5		(257–274)
14	1386.7	1386.4	1386.5	1386.2		(215–227)
	2473.9	2473.5	2473.8	2473.9		(233–256)
15	3079.8	3079.6	3079.5	3079.4		(518–545)
	3320.9	3320.8	3321.0	3320.8	HDSGDQDINVVSGY	(518–547)
	3468.2	3467.9	3467.7	3467.8		(518–548)
16	1505.0	1504.8	1504.4	1504.7		(286–297)
17	1722.0	1722.1	1722.3	1722.4	XELTILHTNDV . . .	(27–40)
18	1345.6	1345.5	1345.7	1345.4	EVNFPILSAN . . .	(134–145)
19	2827.4	2827.2	–	2827.6		(27–50)
20	4302.3	4302.7	4302.6	4302.5	AFDDTVHRY . . .	(434–471)
21	1750.7	1750.9	1751.3	1750.8		(163–179)
22	1939.6	1939.8	1939.9	1939.7	IIALGHSGF . . .	(215–232)
23	2281.6	2281.7	–	2281.5		(495–515)
24	6082.8	6082.9	6083.4	6083.1	TIVYLDGTAQSXRFREXNM . . .	(342–395), Cys^{353}–Cys^{358}, Cys^{365}–Cys^{387}
	6090.5	6090.4	6090.6	6090.5	HPDEMSXNHVSMXIL . . .	(342–374) + (375–395), Cys^{353}–Cys^{358}, Cys^{365}–Cys^{387}
	6108.3	6108.2	6108.7	6108.5	EXNMGNLIXDAM . . .	(342–356) + (357–374) + (375–395), Cys^{353}–Cys^{358}, Cys^{365}–Cys^{387}
25	3005.5	3005.2	3005.5	–	ETPFLSNPGTNL . . .	(180–206)
26	2766.1	2766.3	2766.6	2766.5		(74–97)
	2922.6	2922.4	2922.8	2922.1		(73–97)
	–	3915.6	3915.9	–		(180–214)
27	1909.3	1909.1	1909.6	1909.4	VILPSFLVSGGD . . .	(495–512)
28	–	3246.3	3246.7	3246.9	ETPFLSNPG . . .	(180–208)
29	See Figure 5				NXGTITXENLAAVLPF . . .	(402–427) glycopeptide, Asn^{403}
30	3878.1	3877.9	3878.5	3878.4	EVPAGQYPFIV . . .	(257–291)

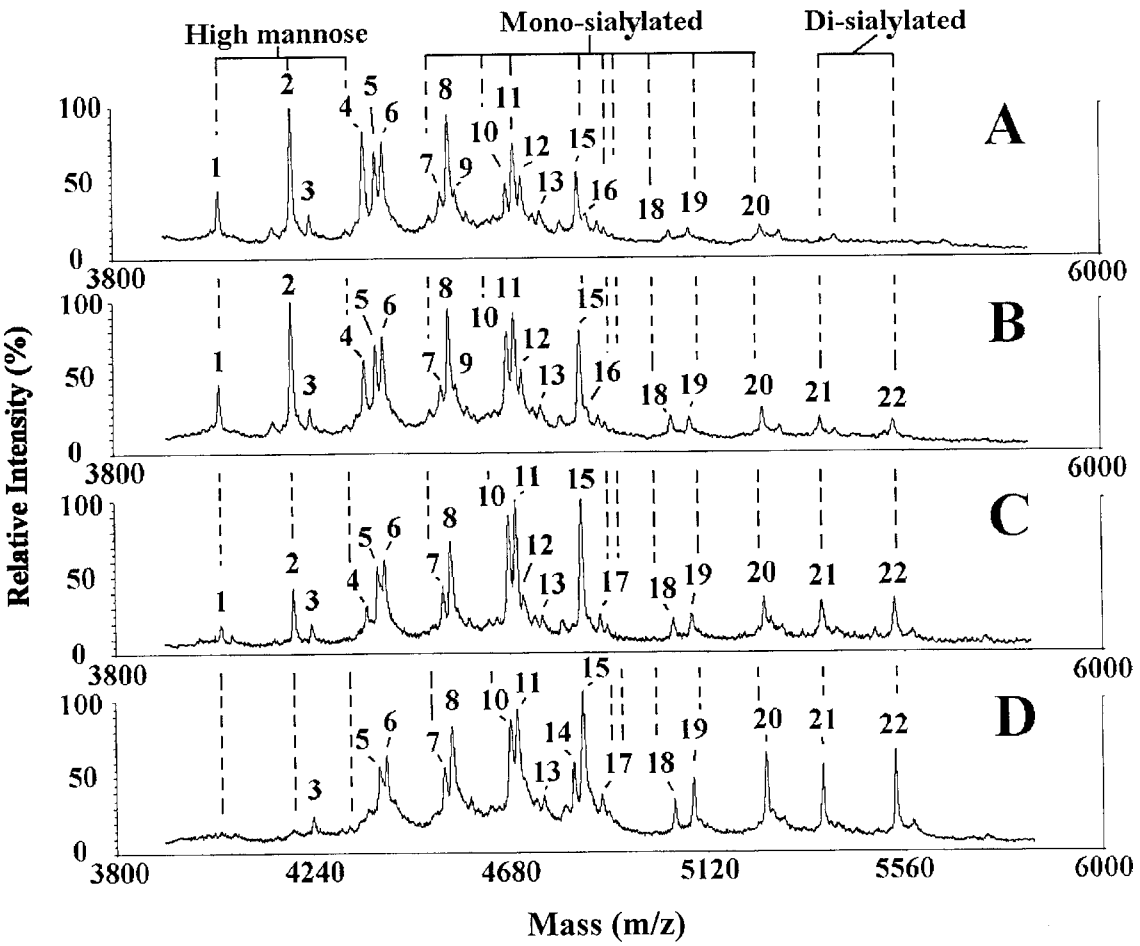

Figure 5 MALDI-MS analysis of the RP-HPLC purified glycopeptides (402–427) occurring in the tryptic digest of the 5′-NT species

(**A**), (**B**), (**C**) and (**D**) correspond to 5′-NT-1, 5′-NT-2, 5′-NT-3 and 5′-NT-4 respectively. Spectra were recorded in negative polarity by using the instrument in linear mode. Each glycopeptide species is numbered and the corresponding structure is reported in Table 5. Signals associated with high mannose, mono- and disialylated glycopeptides are indicated.

DISCUSSION

A soluble form of ecto-5′-NT devoid of the GPI anchor was purified from bull seminal plasma and characterized. When we compared the properties of this enzyme with its GPI-containing counterpart, major differences were observed in (i) post-translational modifications, (ii) molecular aggregation patterns, and (iii) enzymic activity.

Mass-spectrometric investigations revealed that the differences in the post-translational modifications are concerned mainly with the nature of glycan moieties occurring at Asn^{403} and the absence of the GPI anchor at the C-terminus. This absence is not caused by the action of an endogenous PI-PLC but by the activity of a proteolytic enzyme hydrolysing the polypeptide chain at Gln^{547} and/or Phe^{548}. This finding opens a new scenario for the function of 5′-NT as well as on the regulation of its activity. Most of the structures occurring at Asn^{403} in soluble 5′-NT have been already identified in other proteins isolated from the urogenital region in bovine, mouse and human species [24]. This suggests a hypothetical relationship between the nature of the glycan moiety and specialized biological functions of 5′-NT, with respect to the biochemistry of the cell surface as well as to the interaction of the cell with the extracellular matrix. It has already been shown that ecto-5′-NT interacts specifically with the glycoproteins of the extracellular matrix laminin and fibronectin, affecting different cell functions like proliferation, spreading or migration [25]. The soluble ecto-5′-NT, however, would be free to migrate through the extracellular matrix to reach specific sites involved in specialized activities. In this respect, soluble 5′-NT in seminal plasma may be involved in processing reactions on the sperm-surface membrane as part of the capacitation process before fertilization [26].

The GPI-anchored enzyme has been demonstrated to form molecular aggregates in detergent-free media, whereas in the presence of detergents it occurs as a stable dimeric form. Soluble ecto-5′-NT, on the other hand, shows a remarkably low level of aggregation in detergent-free solutions and retains AMPase activity for many months at 4 °C, apparently as a trimer as ascertained by gel-filtration chromatography. Addition of detergents is actually detrimental causing a loss of AMPase activity within a few days. Soluble ecto-5′-NT, therefore, is more suitable than its GPI-containing counterpart for functioning in the extracellular environment.

Enzyme activity of soluble ecto-5′-NT is somewhat different from that of GPI-anchored ecto-5′-NT in that AMP is not the preferred substrate. Furthermore, the K_m values for the substrates tested are 5–10 times higher than those observed previously for the GPI-anchored enzyme. The isotypes obtained following chromatofocusing differed in their measured biological activity. To correlate these findings to specific molecular properties of

Table 5 MALDI-MS analysis of the RP-HPLC-purified glycopeptide (402–427) occurring in the tryptic digest of the isochromatofocusing-separated 5′-NT species

DeoxyHex, deoxyhexose; Hex, hexose; HexNAc, *N*-acetyl-hexosamine; $(Man)_3(GlcNAc)_2$, pentasaccharide core; NeuAc, sialic acid.

Component	5′-NT-1 MH^-	5′-NT-2 MH^-	5′-NT-3 MH^-	5′-NT-4 MH^-	Glycan composition	Structures
1	4035.7	4035.9	4035.6	–	$(Hex)_2 + (Man)_3(GlcNAc)_2$	High mannose
2	4197.6	4197.4	4197.7	–	$(Hex)_3 + (Man)_3(GlcNAc)_2$	High mannose
3	4238.7	4238.9	4238.6	4238.7	$(Hex)_2(HexNAc)_1 + (Man)_3(GlcNAc)_2$	Hybrid
4	4360.1	4360.2	4359.8	–	$(Hex)_4 + (Man)_3(GlcNAc)_2$	High mannose
5	4384.9	4384.7	4384.6	4385.0	$(Hex)_2(HexNAc)_1(DeoxyHex)_1 + (Man)_3(GlcNAc)_2$	Hybrid
6	4401.0	4401.2	4401.3	4400.9	$(Hex)_3(HexNAc)_1 + (Man)_3(GlcNAc)_2$	Hybrid
7	4529.4	4529.2	4529.6	4529.7	$(Hex)_2(HexNAc)_1(NeuAc)_1 + (Man)_3(GlcNAc)_2$	Hybrid
8	4546.4	4546.3	4546.0	4546.5	$(Hex)_3(HexNAc)_1(DeoxyHex)_1 + (Man)_3(GlcNAc)_2$	Hybrid
9	4562.7	4562.9	–	–	$(Hex)_4(HexNAc)_1 + (Man)_3(GlcNAc)_2$	Hybrid
10	4675.4	4675.6	4675.3	4675.7	$(Hex)_2(HexNAc)_2(DeoxyHex)_1(NeuAc)_1 + (Man)_3(GlcNAc)_2$	Complex
11	4691.7	4691.5	4691.9	4692.0	$(Hex)_3(HexNAc)_1(NeuAc)_1 + (Man)_3(GlcNAc)_2$	Hybrid
12	4708.6	4708.3	4708.5	–	$(Hex)_4(HexNAc)_1(DeoxyHex)_1 + (Man)_3(GlcNAc)_2$	Hybrid
13	4750.2	4750.4	4750.0	4750.6	$(Hex)_3(HexNAc)_2(DeoxyHex)_1 + (Man)_3(GlcNAc)_2$	Hybrid
14	–	–	–	4816.3	$(HexNAc)_4(DeoxyHex)_2 + (Man)_3(GlcNAc)_2$	Complex
15	4838.0	4838.3	4838.0	4838.4	$(Hex)_3(HexNAc)_1(DeoxyHex)_1(NeuAc)_1 + (Man)_3(GlcNAc)_2$	Hybrid
16	4854.1	4854.0	–	–	$(Hex)_4(HexNAc)_1(NeuAc)_1 + (Man)_3(GlcNAc)_2$	Hybrid
17	–	–	4878.7	4878.5	$(Hex)_2(HexNAc)_2(DeoxyHex)_1(NeuAc)_1 + (Man)_3(GlcNAc)_2$	Complex
18	4977.4	4977.6	4977.3	4977.0	$(Hex)_1(HexNAc)_4(NeuAc)_1 + (Man)_3(GlcNAc)_2$	Complex
19	5041.6	5041.3	5041.7	5041.2	$(Hex)_3(HexNAc)_2(DeoxyHex)_1(NeuAc)_1 + (Man)_3(GlcNAc)_2$	Hybrid
20	5244.3	5244.6	5244.3	5244.5	$(Hex)_3(HexNAc)_3(DeoxyHex)_1(NeuAc)_1 + (Man)_3(GlcNAc)_2$	Complex
21	–	5373.4	5373.5	5373.0	$(Hex)_2(HexNAc)_3(DeoxyHex)_1(NeuAc)_2 + (Man)_3(GlcNAc)_2$	Complex
22	–	5535.0	5534.9	5535.5	$(Hex)_3(HexNAc)_3(DeoxyHex)_1(NeuAc)_2 + (Man)_3(GlcNAc)_2$	Complex

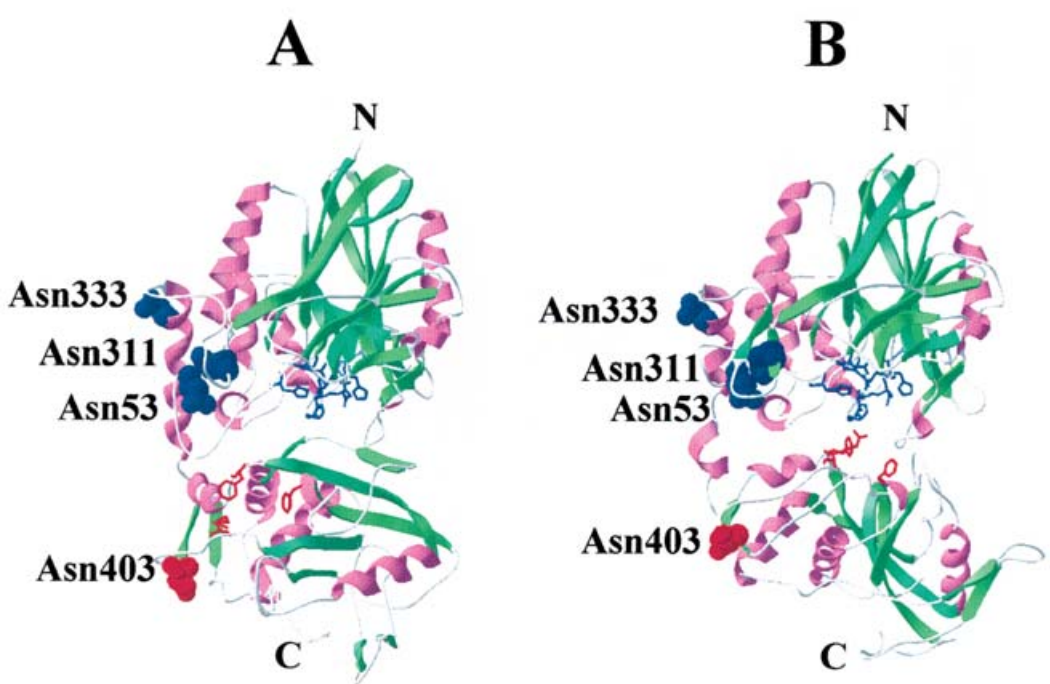

Figure 6 Three-dimensional model of bovine-soluble 5′-NT in open (A) and closed (B) conformation

Helices and β-strands are coloured in magenta and green respectively. Atoms of the four glycosylation sites are shown by spheres, coloured differently depending on their occurrence at the N-terminus (blue) or C-terminus (red) respectively. The residues present in the active site of the enzyme (Asp^{36}, His^{38}, Asp^{85}, Asn^{117}, His^{118}, Asp^{121}, His^{220} and His^{243}) and in the substrate-binding pocket (Arg^{395}, Phe^{417} and Phe^{500}) are indicated with stick representation and are coloured in blue and red respectively.

bovine 5′-NT, three-dimensional models of the monomer were constructed on the basis of the crystallographic structures of the *E. coli* enzyme [27–29]. Sequence identity between the two polypeptides was approx. 23%. The present study enabled models to be constructed for the open and closed conformation of the enzyme as reported for the *E. coli* protein [27–29]. As illustrated in Figure 6, the structure presents an N-terminal domain (Trp^{27}-Val^{329}) and a C-terminal domain (Gln^{351}-Ser^{549}) connected by a long α-helix. Each domain contains a four-layered structure made up of α/β-β-β-α (N) and α/β-β-α-β (C) motifs respectively, with a core rich in β-sheets. Loop regions between β1-α1, β5-β6, β19-β20, β23-β24 and β24-β25 were longer

in the bovine enzyme with respect to *E. coli*. Conversely, loops between β10-α7 and β17-α8 were shorter. Disulphide bridges between Cys^{51}-Cys^{57}, Cys^{353}-Cys^{358}, Cys^{365}-Cys^{387} and Cys^{476}-Cys^{479} (conserved in all mammalian enzymes) were located in loop regions. These disulphides are absent from the bacterial enzymes that conversely present a unique bridge Cys^{258}-Cys^{275} not occurring in the mammalian counterparts. With the only exception of Asn^{245}, all residues hypothesized to be present in the active site of the bovine enzyme Asp^{36}, His^{38}, Asp^{85}, Asn^{117}, His^{118}, Asp^{121}, His^{220} and His^{243} are conserved in the *E. coli* protein. The side chains of these amino acids are capable of co-ordinating the two zinc ions, which have been shown to be essential for the activity of the bovine enzyme [30]. In contrast with the above, only three of the five residues present in the substrate-binding pocket of the microbial protein are conserved in the bovine counterpart (Arg^{395}, Phe^{417} and Phe^{500}). These residues are subjected to approx. 20 Å motion in the interconversion from the open (inactive) to the closed (active) conformation of the *E. coli* enzyme (see Figure 6). This conversion resulted from a 95 ° hinge-bending rotation occurring between the two domains. Only one of the two residues (Lys^{341}) hypothesized as forming the core of the hinge region is conserved in the *E. coli* protein.

The four glycosylation sites occurring in the bovine protein are all located along one face of the molecule and could conceivably modulate aggregation phenomena with other macromolecules. Three Asn residues presenting N-linked high mannose saccharides are located in the N-terminal domain, whereas Asn^{403}, with its mixture of heterogeneous N-linked oligosaccharides (high mannose, complex and hybrid structures), is present in the C-terminal domain. In the model presenting an open conformation, this amino acid residue is positioned close to the substrate-binding pocket (Figure 6A). Therefore steric hindrance and charge of the bound oligosaccharides could affect nucleotide recognition. This hypothesis could explain the different biological activities measured for the four species obtained following chromatofocusing separation. These components differ by an increase in sialylated and disialylated oligosaccharides and change in K_m values. However, other effects, such as aggregation state properties, also need to be considered in explaining the differences observed with respect to GPI-bound 5′-NT. It is reasonable to speculate that the biological activity of 5′-NT is modulated by post-translational processing of its polypeptide chain.

We thank Dr Roy Jones (The Babraham Institute, Babraham Hall, Babraham, Cambridge, U.K.), for his helpful suggestions and revision of the manuscript. This work was supported by funds from the Consiglio Nazionale delle Ricerche and by the EC project "Valorizzazione Prodotti Tipici Mediterranei" (Fondi Strutturali, Assegnazione 104131).

REFERENCES

1 Zimmermann, H. (1992) 5′-nucleotidase: molecular structure and functional aspects. Biochem. J. **285**, 345–365
2 Obata, T., Kubota, S. and Yamanaka, Y. (2001) Histamine increases interstitial adenosine concentration via activation of ecto-5′-nucleotidase in rat hearts *in vivo*. J. Pharmacol. Exp. Ther. **298**, 71–76
3 Sato, T., Obata, T., Yamanaka, Y. and Arita, M. (2000) Nicorandil increases adenosine 5′-monophosphate-primed interstitial adenosine via activation of ecto-5′-nucleotidase in rat hearts. Heart Vessels **15**, 81–85
4 Zou, A. P., Wu, F., Li, P. L. and Cowley, Jr, A. W. (1999) Effect of salt loading on adenosine metabolism and receptor expression in renal cortex and medulla in rats. Hypertension **33**, 511–516
5 Lara, D. L., Vianna, M. R., deParis, F., Quevedo, J., Oses, J. P., Battastini, A. M., Sarkis, J. J. and Souza, D. O. (2001) Chronic treatment with clozapine, but not haloperidol, increases striatal ecto-5′-nucleotidase activity in rats. Neuropsychobiology **44**, 99–102
6 Wortmann, R. L., Veum, J. A. and Rachow, J. W. (1991) Synovial fluid 5′-nucleotidase activity. Relationship to other purine catabolic enzymes and to arthropathies associated with calcium crystal deposition. Arthritis Rheum. **34**, 1014–1120
7 Klemens, M. R., Sherman, W. R., Holmberg, N. J., Ruedi, J. M., Low, M. G. and Thompson, L. F. (1990) Characterization of soluble vs membrane-bound human placental 5′-nucleotidase. Biochem. Biophys. Res. Commun. **172**, 1371–1377
8 Letho, M. T. and Sharon, F. J. (1998) Release of the glycosylphosphatidylinositol-anchored enzyme ecto-5′-nucleotidase by phospholipase C: catalytic activation and modulation by the lipid bilayer. Biochem. J. **332**, 101–109
9 Fini, C., Amoresano, A., Andolfo, A., D'Auria, S., Floridi, A., Paolini, S. and Pucci, P. (2000) Mass spectrometry study of ecto-5′-nucleotidase from bull seminal plasma. Eur. J. Biochem. **267**, 4978–4987
10 Fini, C., Coli, M., Floridi, A., D'Auria, S., Staiano, M., Nucci, R. and Rossi, M. (1998) Temperature effects on the structural and functional properties of GPI-anchored and anchor-less bull seminal plasma ecto-5′-nucleotidase. J. Biochem. **123**, 269–274
11 Shevchenko, A., Wilm, M., Vorm, O. and Mann, M. (1996) Mass spectrometric sequencing of proteins from silver-stained polyacrylamide gels. Anal. Chem. **68**, 850–858
12 Gorg, A., Postel, W. and Gunther, S. (1988) The current state of two-dimensional electrophoresis with immobilized pH gradients. Electrophoresis **9**, 531–546
13 Laemmli, U. K. (1970) Cleavage of structural proteins during the assembly of the head of bacteriophage T4. Nature (London) **227**, 680–685
14 Krause, I., Buchberger, J., Weiss, G., Pflugler, M. and Klostermeyer, H. (1988) Isoelectric focusing in immobilized pH gradients with carrier ampholytes added for high-resolution phenotyping of bovine β-lactoglobulins: characterization of a new genetic variant. Electrophoresis **9**, 609–613
15 Appel, R. D. and Hochstrasser, D. F. (1999) Computer analysis of 2-D images. Methods Mol. Biol. **112**, 363–381
16 Allegrini, S., Scaloni, A., Ferrara, L., Pesi, R., Pinna, P., Sgarrella, F., Camici, M., Eriksson, F. and Tozzi, M. G. (2001) Bovine cytosolic 5′-nucleotidase acts through the formation of an aspartate 52-phosphoenzyme intermediate. J. Biol. Chem. **276**, 33526–33532
17 Damer, C., Partridge, J., Pearson, W. R. and Haystead, T. A. (1998) Rapid identification of protein phosphatase 1-binding proteins by mixed peptide sequencing and data base searching. J. Biol. Chem. **273**, 24396–24405
18 Barton, G. J. (1990) Protein multiple sequence alignment and flexible pattern matching. Methods Enzymol. **183**, 403–428
19 Barton, G. J. and Sternberg, M. J. E. (1987) Evaluation and improvements in the automatic alignment of protein sequences. Protein Eng. **1**, 89–94
20 Doreleijers, J. F., Vriend, G., Raves, M. L. and Kaptein, R. (1999) Validation of nuclear magnetic resonance structures of proteins and nucleic acids: hydrogen geometry and nomenclature. Proteins: Struct. Funct. Genet. **37**, 404–416
21 Guex, N. and Peitsch, M. C. (1997) SWISS-MODEL and the Swiss-PdbViewer: an environment for comparative protein modeling. Electrophoresis **18**, 2714–2723
22 Wetlaufer, D. B. (1962) Ultraviolet spectra of proteins and amino acids. In Advances in Protein Chemistry, vol. 17 (Anfinsen, Jr, C. B., Anson, M. L., Bailey, K. and Edsall, J. T., eds.), pp. 304–383, Academic Press, New York and London
23 Taguchi, R., Hamakawa, N., Maekawa, N. and Ikezawa, H. (1999) Application of ESI MS/MS and MALDI–TOF-MS to structural analysis of the glycosyl-phosphatidylinositol-anchored protein. J. Biochem. (Tokyo) **126**, 421–429
24 Cooper, C. A., Harrison, M. J., Wilkins, M. R. and Packer, N. H. (2001) GlycoSuiteDB: a new curated relational database of glycoprotein glycan structures and their biological sources. Nucleic Acids Res. **29**, 332–335
25 Stochaj, U., Dieckhoff, J., Mollenhauer, J., Cramer, M. and Mannherz, H. G. (1989) Evidence for the direct interaction of chicken gizzard 5′-nucleotidase with laminin and fibronectin. Biochim. Biophys. Acta **992**, 385–392
26 Schiemann, P. J., Aliante, M., Wennemuth, G., Fini, C. and Aumüller, G. (1994) Distribution of endogenous and exogenous 5′-nucleotidase in bovine spermatozoa. Histochemistry **101**, 253–262
27 Knöfel, T. and Sträter, N. (1999) X-ray structure of the *Escherichia coli* periplasmic 5′-nucleotidase containing a dimetal catalytic site. Nat. Struct. Biol. **6**, 448–453
28 Knöfel, T. and Sträter, N. (2001) Mechanism of hydrolysis of phosphate esters by the dimetal center of 5′-nucleotidase based on crystal structures. J. Mol. Biol. **309**, 239–254
29 Knöfel, T. and Sträter, N. (2001) *E. coli* 5′-nucleotidase undergoes a hinge-bending domain rotation resembling a ball-and-socket motion. J. Mol. Biol. **309**, 255–266
30 Fini, C., Palmerini, C. A., Damiani, P., Stochaj, U., Mannherz, H. G. and Floridi, A. (1990) 5′-nucleotidase from bull seminal plasma, chicken gizzard and snake venom is a zinc metalloprotein. Biochim. Biophys. Acta **1038**, 18–22

Received 29 October 2002/11 February 2003; accepted 27 February 2003
Published as BJ Immediate Publication 27 February 2003, DOI 10.1042/BJ20021687